Biophysical Journal Volume 89 October 2005 2443–2457

Caveolin-1 Expression and Membrane Cholesterol Content Modulate N-Type Calcium Channel Activity in NG108-15 Cells

M. Toselli,* G. Biella,* V. Taglietti,* E. Cazzaniga,† and M. Parenti†

*Department of Cellular and Molecular Physiological and Pharmacological Sciences, and INFM (National Institute of Matter Physics), University of Pavia, Pavia, Italy; and †Department of Experimental and Environmental Medicine and Medical Biotechnologies, University of Milano-Bicocca, Monza, Italy

ABSTRACT Caveolins are the main structural proteins of glycolipid/cholesterol-rich plasmalemmal invaginations, termed caveolae. In addition, caveolin-1 isoform takes part in membrane remodelling as it binds and transports newly synthesized cholesterol from endoplasmic reticulum to the plasma membrane. Caveolin-1 is expressed in many cell types, including hippocampal neurons, where an abundant SNAP25-caveolin-1 complex is detected after induction of persistent synaptic potentiation. To ascertain whether caveolin-1 influences neuronal voltage-gated Ca^{2+} channel basal activity, we stably expressed caveolin-1 into transfected neuroblastoma × glioma NG108-15 hybrid cells [cav1(+) clone] that lack endogenous caveolins but express N-type Ca^{2+} channels upon cAMP-induced neuronal differentiation. Whole-cell patch-clamp recordings of cav1(+) cells demonstrated that N-type current density was reduced in size by ~70% without any significant change in the time course of activation and inactivation and voltage dependence. Moreover, the cav1(+) clone exhibited a significantly increased proportion of membrane cholesterol compared to wild-type NG108-15 cells. To gain insight into the mechanism underlying caveolin-1 lowering of N-current density, and more precisely to test whether this was indirectly caused by caveolin-1-induced enhancement of membrane cholesterol, we compared single N-type channel activities in cav1(+) clone and wild-type NG108-15 cells enriched with cholesterol after exposure to a methyl-β-cyclodextrin-cholesterol complex. A lower Ca^{2+} channel activity was recorded from cell-attached patches of both cell types, thus supporting the view that the increased proportion of membrane cholesterol is ultimately responsible for the effect. This is due to a reduction in the probability of channel opening caused by a significant decrease of channel mean open time and by an increase of the frequency of null sweeps.

INTRODUCTION

Upon cell extraction with nonionic detergents, such as Triton X-100, and ultracentrifugation, membranes can be separated into an insoluble fraction, containing detergent-insoluble domains enriched with glycosphingolipids and cholesterol (DIGs), and a soluble phospholipid-rich fraction containing the bulk of cellular membranes. Subsets of DIGs can be distinguished in certain cell types, i.e., planar lipid rafts and invaginated caveolae, containing caveolins as main structural protein components. A number of signaling molecules, including receptors, effectors, and modulatory proteins, are concentrated in DIGs. Numerous laboratories have demonstrated localization of proteins in caveolae, interaction of these proteins with caveolins, and the ability of overexpressed caveolins or peptides derived from caveolins to suppress or stimulate signaling functions in vitro or in cultured cells (1–3). A subcellular localization of ion channels in caveolae and a modification of their gating properties after changes in membrane cholesterol have been described as well (4). Indeed, the relationship of caveolin to cholesterol is of considerable interest: caveolin-1 binds cholesterol and also increases cholesterol transport from endoplasmic reticulum to plasma membrane, suggesting a primary role for caveolin in cholesterol regulation. Therefore, it is not unexpected that ion channels, proteins designed to surmount the impermeability of the surface membrane, might be functionally dependent on the constituent lipids of the membrane itself. If alterations in membrane composition by depletion of lipids enriched in rafts and/or caveolae have significant effects on channel function, this could translate into large changes in cellular excitability (5). However, it remains unclear whether these effects are due to direct protein-lipid interactions or indirect signaling mechanisms. Certainly, changes in membrane cholesterol can directly modulate ion channel function (6,7). In addition, rafts might have unique biophysical properties that directly affect channel function. Some of these parameters include lateral pressure profile, bilayer fluidity, bilayer thickness, and surface charge (8). Lipid raft-channel association might also function as a mechanism of cell-surface compartmentation.

In a previous report, we showed that caveolin-1 expression attenuates the G-protein-mediated down-modulation of voltage-gated N-type Ca^{2+} channel currents (9). The study described here focused on possible functional effect(s) of caveolin-1 on the basal activity of N-type Ca^{2+} channels, independent of G-protein activation. This might be physiologically relevant considering that in neurons, the activation of the voltage-gated N-type calcium channel plays a significant role in multiple cellular functions including neurotransmitter release, regulation of gene expression, dendritic development, and

Submitted May 5, 2005, and accepted for publication July 1, 2005.

Address reprint requests to Mauro Toselli, Dept. of Cellular and Molecular Physiological and Pharmacological Sciences, University of Pavia, Via Forlanini 6, I-27100 Pavia, Italy. Tel.: 39-0382-987612; Fax: 39-0382-987527; E-mail: mtoselli@unipv.it.

0006-3495/05/10/2443/15 $2.00

doi: 10.1529/biophysj.105.065623

synaptic plasticity. In addition, caveolin-1 has been detected in neurons and neuronal cell lines (10). Most importantly, recent findings show that after the induction of persistent synaptic potentiation, an abundant 40-kDa SNAP25-caveolin-1 complex can be measured in hippocampal neurons (11).

For our investigation we used the stably expressing recombinant caveolin-1 clone cav1(+) (9), obtained by the NG108-15 cell line, lacking endogenous caveolins and caveolae (12). Upon in vitro differentiation, NG108-15 cells acquire a neuron-like phenotype and express N-type Ca^{2+} channels (13). These features make these cells an ideal model to investigate whether caveolin-1 plays any role in the regulation of N-type Ca^{2+} channel basal activity.

We show here that the N-type current density is attenuated in NG108-15 cells expressing recombinant caveolin-1. The mechanism of this N-current depression has been investigated as well and the possibility of a direct interaction of the channel with caveolin-1 through its scaffolding was considered first. Considering that caveolin-1 is also a cholesterol-binding protein that delivers cholesterol from the endoplasmic reticulum to the plasmalemma, another putative action of caveolins could be to regulate plasma membrane proteins indirectly by modulating the cholesterol content of lipid raft domains and/or caveolae (14). This second hypothesis has been considered as well since in the cav1(+) clone an increase of the amount of membrane cholesterol was observed and in control cells the N-current density depression could be mimicked by application of exogenous cholesterol.

These results may be useful in making predictions about the effects of endogenous caveolins in neurons, where they might significantly influence voltage-gated Ca^{2+} channel activity and thereby all physiological effects mediated by an increase in intracellular Ca^{2+}.

MATERIALS AND METHODS

Cell culture

Mouse neuroblastoma × rat glioma NG108-15 hybrid cells were grown as monolayers in Dulbecco's modified Eagle's medium (DMEM), 10% heat inactivated fetal calf serum, hypoxantine-aminopterin-thymidine supplement, 100 μg streptomycin/ml, and 100 IU penicillin/ml in a 5% CO_2-humidified atmosphere at 37°C. The NG108-15 clones constitutively expressing recombinant caveolin-1 [cav1(+)] and transfected with empty vector [cav1(−)] were obtained as previously described (9) and constantly maintained in a medium supplemented with 400 μg/ml hygromycin B (Roche) selection antibiotic. All cells were grown in plastic flasks, and plated onto plastic Petri dishes for use in electrophysiological experiments. The culture medium was replaced three times per week.

To induce cell differentiation into a neuronal phenotype and Ca^{2+} channel expression (13), 10 μM prostaglandin E_1 (ICN Biochemicals, Milan, Italy), and 1 mM theophylline were added to the culture medium at least 5 days before electrophysiological recordings.

Cholesterol enrichment

To enhance the cellular cholesterol content, cultures were exposed to a methyl-β-cyclodextrin (MβCD; Sigma Chemical, St. Louis, MO) solution saturated with cholesterol (Sigma Chemical) at a MβCD/cholesterol molar ratio of 8:1, prepared as described by Levitan and colleagues (15). Briefly, cholesterol was stored as a stock solution in chloroform/methanol (1:1 v/v). The required amount of cholesterol was transferred to a glass tube and left at room temperature until the solvent was completely evaporated. Then 5 mM MβCD solution in serum-free DMEM was added to the dried cholesterol, and the tube was vortexed, sonicated, and incubated overnight in a rotating bath at 37°C. The resulting cholesterol-saturated MβCD mixture was diluted in serum-free DMEM to obtain the final working cholesterol concentrations of 50 and 5 μg/ml. Before each experiment, cells were washed three times with serum-free DMEM and incubated for 120 min with the cholesterol/MβCD solution in a humidified CO_2 incubator at 37°C. After exposure to cholesterol/MβCD, cells were washed three times with serum-free DMEM. Control cells were treated similarly and incubated with serum-free DMEM solution without any MβCD.

Lipid extraction and analysis

Total cell lipids were extracted from pelleted cells and partitioned into an organic and an aqueous phase, according to Giglioni et al. (16). Protein assay was performed on the delipidized protein pellet according to a modified Lowry protocol (17) using bovine serum albumin as a standard. Lipids in the organic phase were separated by high-performance thin-layer chromatography (HPTLC) using, as the solvent system, chloroform/methanol/acetic acid/H_20 60:45:4:2 v/v/v/v for phospholipids, and hexane/diethylether/acetic acid 20:35:1 v/v/v for cholesterol, and then sprayed with anisaldehyde reagent. After heating the plate at 180°C for 15 min, the HPTLC plates were submitted to densitometric scanning of the visualized bands. Quantification was made on the basis of known amounts of standard lipids loaded on the same plate. Cholesterol amounts are expressed as nanomoles of steroid per nanomole of phospholipids. Silica gel precoated thin-layer plates (HPTLC Kieselgel 60) and solvents were from Merck (Darmstadt, Germany).

Solutions for electrophysiology

During whole-cell recording, seals between electrodes and cells were established in a solution containing (mM/L): 135 NaCl, 1.8 $CaCl_2$, 5.5 KCl, 10 glucose, and 10 HEPES/NaOH (pH 7.4). This extracellular saline was maintained for Kv-current recording. After establishing the whole-cell configuration, and for Ba^{2+}-current recording, cells were perfused with an external saline containing (mM/L): 135 NaCl, 10 $BaCl_2$, 10 glucose, 10 HEPES/NaOH (pH 7.4), 1 4-aminopyridine, 10 tetraethylammonium chloride, and 10^{-3} tetrodotoxin (TTX). The patch pipettes were filled with (mM/L): 125 CsCl, 20 tetraethylammonium chloride, 10 EGTA, 1 $MgCl_2$, 4 Mg-ATP, and 10 HEPES/CsOH (pH 7.4). Most differentiated NG108-15 cells expressed low-voltage-activated T-type, and high-voltage-activated L- and N-type Ca^{2+} channels (13,18). N-type currents were isolated by cell application of 10 μM nifedipine (Bayer AG, Wuppertal, Germany) dissolved in the external saline to block L-type channels, and by holding the membrane potential of the cell at −40 mV to inactivate T-type Ca^{2+} currents. For L-type Ba-current recording, extracellular nifedipine was substituted with 10 μM ω-conotoxin GVIA (Alomone Labs, Jerusalem, Israel). For Kv-current recording, the pipette-filling solution contained (in mM/L): 140 KCl, 4 NaCl, 0.02 $CaCl_2$, 0.8 EGTA, 2 $MgCl_2$, 4 Mg-ATP, and 10 HEPES/KOH (pH 7.4). External solutions were exchanged using a fast multibarrel delivery system positioned close to the recorded cells.

For the cell-attached recordings, the pipette control solution contained (mM/L): 100 $BaCl_2$, 10 TEA-Cl, 1 $MgCl_2$, and 10 Na-HEPES, plus 10 μM nifedipine and 300 nM TTX (pH 7.3 with TEA-OH). Membrane potential was zeroed with a solution containing (mM/L): 135 potassium aspartate, 1 $MgCl_2$, 10 HEPES, and 5 EGTA, plus 300 nM TTX (pH 7.3 with KOH).

The caveolin scaffolding peptide was a gift from Dr. Sessa (Dept. of Pharmacology, Yale University, New Haven, CT). It corresponds to the putative scaffolding domain of caveolin-1 (amino acids 82–101; DGIWKASFTTFTVTKYWFYR). Stock solutions (10 mM) of the peptide in DMSO

were stored in aliquots at −20°C and diluted into the patch pipette saline to a final concentration of 10 μM.

Current recordings and data analysis

Patch pipettes were made from borosilicate glass tubing (Hilgenberg, Malsfeld, Germany) and fire-polished to a final resistance of 0.5–2.0 MΩ when filled with internal solutions. For cell-attached recording pipette tips were coated with Sylgard to reduce capacitance and noise. All the experiments were performed at room temperature (22–24°C).

Whole-cell and single-channel currents were recorded with an Axopatch 200A amplifier (Axon Instruments, Burlingame, CA) digitized at sampling intervals of 26–100 μs using a DigiData 1200 (Axon Instruments) for single-channel recordings. Stimulation, acquisition, and data analysis were carried out with PCLAMP (Axon Instruments) and ORIGIN (Microcal Software, Northampton, MA) software. Fast capacitive transients were reduced on-line by analog circuitry. Residual capacitive and leak currents were removed by P/4 subtraction for whole-cell recordings, whereas for single-channel recordings they were removed by subtracting from each active sweep an idealized current obtained by fitting the averaged silent traces (nulls) with a multi-exponential function. Currents were filtered at 3 KHz. Current density was calculated by dividing the peak or steady-state current amplitude by membrane capacitance. Membrane capacitance was calculated by dividing the integral of the uncompensated capacitive current (the capacitive charge movement) produced by a voltage step of −10 mV by the amplitude of the voltage step itself.

Single-channel event detection was performed with the 50% threshold detection method and limited to those patches containing only one channel. Such patches were identified for the absence of overlapping unitary currents at +40 mV, at which the probability of channel opening is relatively high and multiple open levels could be clearly resolved when present. Furthermore, the following algorithm was applied to estimate the likelihood of single-channel activity in those patches without superimposed openings (19): $P_2(T) = 1 - (1 - P_{2o})^{T/t}$, where $P_2(T)$ is the cumulative probability of observing superimposed openings due to the activity of two identical channels during the total observation time T, P_{2o} is the overall probability of finding two simultaneous openings, and t is twice the mean open time. The patches used for further analysis were those with $P_2(T) > 0.999$ despite the absence of superimposed openings during the observation time T.

As specified in the text, open probability (P_o) was evaluated either excluding first and last channel closures and null sweeps, or by dividing the sum of the open times by the entire step duration. The first method for calculating P_o ignores the first latency and the rate of channel inactivation and is preferred for looking at changes in P_o when the channel is actively gating. It also furnishes an estimate of P_o independent of the length of the pulse. The mean P_o at each potential was calculated by averaging the P_o measured from each single patch over a variable number of sweeps. To construct $P_o(V)$ curves, mean P_o values were plotted versus potential and fitted to a Boltzmann equation. To estimate the mean open and mean closed times, the single-channel events were log-binned into open and closed time histograms, excluding the first and the last closures and limiting the analysis to events longer than twice the dead time (360 μs) (20). Openings were long enough and well resolved. We followed two ways to determine mean open and mean closed times, obtaining very similar results. In one case, the two parameters were estimated by averaging the arithmetic mean of the open and closed times (t_o and t_c) of each patch. This gave an estimate of the two parameters independent of the fitting procedure and number of exponentials used for the fit, and allowed the derivation of values at various potentials when, for practical reasons, a limited number of sweeps at each potential could be collected (see Figs. 3 *D* and 4 *D*). In the second case, single-channel events at +20 mV were plotted on linear coordinates to construct a single open and closed time distribution which was best fitted with either one or two exponentials using the maximum likelihood method (21). In this case, the distributions were constructed from a large number of traces coming either from many patches with a small number of traces per patch or from fewer patches with many more traces per patch. The mean t_o and mean t_c obtained from the fit had a nice correspondence with those obtained using the first method at the same potential (+20 mV). The open times were well fitted with one exponential, whereas the fit of the closed times required two components.

All data in the text and figures are given as mean ± SE for n observations. Statistical significance (p) was calculated using Student's paired t-test. Fitting of the prepulse/postpulse data was performed by a nonlinear regression method based on the Levenberg-Marquardt algorithm.

Concerning ''runs analysis'', used to test null sweeps for randomness, the distribution of the number of runs was approximated by an asymptotic distribution, forming a standardized random variable, Z, with a mean of zero and variance of 1. For our purposes

$$Z = -[R - 2n\rho(1-\rho)]/[2\sqrt{(n)}\rho(1-\rho)], \qquad (1)$$

where R is the number of runs, n is the total number of trials, and r is the probability of at least one channel opening during a trial. The expected number of runs is $2n\rho(1-\rho)$. Positive values of Z correspond to clustering of sweeps with openings (22).

Simulation of single-channel activity was done by using the program CSIM (Axon Instruments).

RESULTS

Effect of the expression of recombinant caveolin-1 on N-type Ca^{2+} channel currents

In a previous report (9) we showed that the G-protein-mediated down-modulation of N-type Ca^{2+} channel current was attenuated in a NG108-15 cav1(+) clone compared to parental cells, whereas the basal gating properties of channel activation and inactivation did not significantly differ between the two cell types. To follow up that study, here we compare the basal activities of N-type Ca^{2+} channels, independent of G-protein-mediated modulation. Upon inspection of representative sample tracings of superimposed Ba^{2+} currents (normalized to cell capacitance to give current densities), elicited at different test potentials (−20/+20 mV) in wild-type and cav1(+) NG108-15 cells (Fig. 1 *A*), the latter exhibited a sizeable depression of the N-current. Indeed, the mean results of the current-voltage relationships (Fig. 1 *B*) showed an activation threshold at ~−30 mV and a peak at +10 mV in both cell types, but the N-current was strongly depressed within a wide range of test potentials in cav1(+) cells. The average current density measured at +10 mV was −4.28 ± 0.83 pA/pF in wild-type cells ($n = 37$) and 1.12 ± 0.25 pA/pF in cav1(+) cells ($n = 26$), with a net current density decrement of 74% ($p < 0.002$). In contrast, the average current densities measured in cells ($n = 29$) from a cav1(−) clone (obtained by transfection with an empty vector, and used here as a negative control), was not significantly different from that measured in wild-type NG108-15 cells (Fig. 1 *C*). By dividing the N-current density at each test potential by the driving force, we obtained the macroscopic conductance (g) as a function of voltage (V). Fitting the data points of the normalized conductance (obtained by dividing $g(V)$ by the maximum conductance G_{max}) with a Boltzmann equation did not show any significant change in

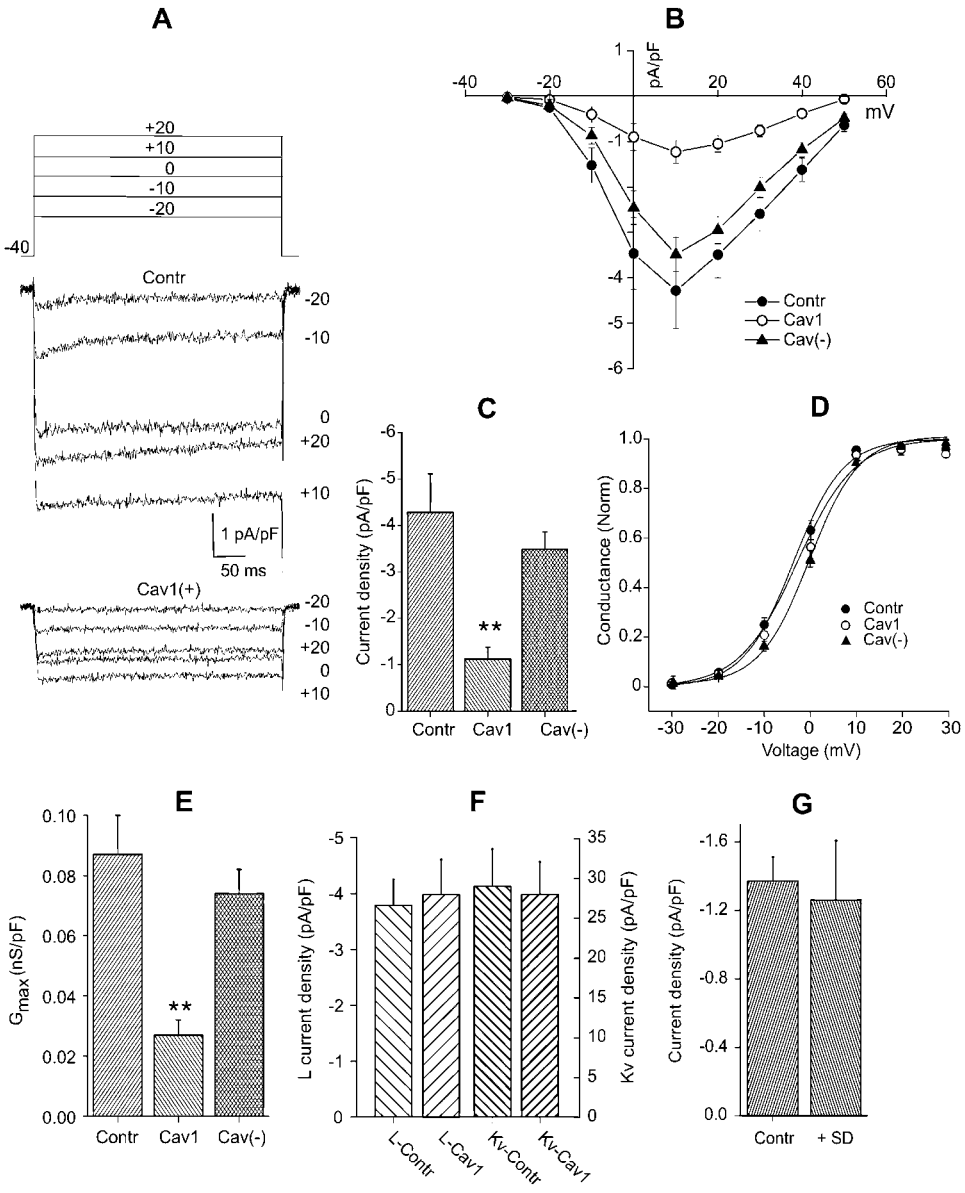

FIGURE 1 N-type Ca^{2+} channel currents in control NG108-15 and in cav1(+) cells. (*A*) Representative Ba^{2+} current density profiles obtained from a normal NG108-15 cell (*Contr*) and a cav1(+) cell (*lower tracings*). Steps of 370-ms duration were applied to increasing test potentials (−20 to +20 mV) from a holding potential of −40 mV. (*B*) Current density-voltage relationship of N-currents from normal NG108-15 (*solid circles*, $n = 15$), cav1(+) (*open circles*, $n = 19$), and cav(−) cells (*triangles*, $n = 29$). (*C*) Average N-current densities in control NG108-15 ($n = 37$), cav1(+) ($n = 26$, $p < 0.002$), and cav(−) cells ($n = 29$) at +10 mV. (*D*) Mean voltage dependence of N-type Ca^{2+} channel conductance (normalized) for wild-type NG108-15 (*solid circles*, $n = 15$), cav1(+) (*open circles*, $n = 19$), and cav(−) cells (*triangles*, $n = 29$). N-type conductance was estimated according to the relation $g = I_{Ba}/(V - V_{Ba})$,where I_{Ba} refers to peak current values and V_{Ba} is the extrapolated reversal potential (+60 mV). The continuous line through data points is the least-squares best fit of the Boltzmann equation $g_{norm} = 1/\{1 + \exp[(V - V_{1/2})/k]\}$, where $V_{1/2}$ and k values were, respectively, −3.7 ± 0.5 mV and 5.4 ± 0.2 mV for wild-type cells, 2.9 ± 0.5 mV and 6.2 ± 0.2 mV for cav1(+) cells, and 0.3 ± 0.3 mV and 5.4 ± 0.3 mV for cav(−) cells. (*E*) Average N-current maximal conductances in wild-type ($n = 15$), cav1(+) ($n = 19$, $p < 0.001$), and cav(−) cells ($n = 29$). (*F*) Current densities from L-type Ca^{2+} channels (*left*) and delayed-rectifier K^+ channels (*right*) in wild-type and cav1(+) cells. (*G*) Current density in wild-type cells ($n = 11$) and in cells dialyzed with 10 μM caveolin-1 scaffolding-domain peptide ($n = 11$).

the slope or any shift of the *g-V* relationship obtained from the cav1(+) clone in comparison to wild-type cells or cav(−) cells (Fig. 1 *D*). By contrast, a significant decrease of G_{max} from 0.087 ± 0.013 nS/pF ($n = 15$) in wild-type cells to 0.027 ± 0.005 nS/pF ($n = 19$) in cav1(+) cells was measured (Fig. 1 *E*). Thus, remarkably lower current density and maximum conductance are detected in cav1(+) cells, suggesting that caveolin-1 has an effect on basal channel activity, seemingly without modifying the voltage-dependence properties of the N-type channel inferred from whole-cell Ba^{2+} current measurements.

To test whether the current depression induced by caveolin-1 is a specific feature of N-type Ca^{2+} channels or is common to other channel types, we compared the current density amplitudes of wild-type and cav1(+) NG108-15 cells for the L-type Ca^{2+} and the delayed rectifier K^+ channels. The results, summarized in the histogram of Fig. 1 *F*, do not evidence any significant difference between wild-type and cav1(+) cells, thus suggesting that caveolin-1 specifically affects Ca^{2+} conductance through N-type channels in NG108-15 cells.

Caveolin-1 has been suggested to negatively regulate signal transduction as a result of the binding of its ''scaffolding domain'' to key signaling molecules, such as G-protein α-subunits, Ha-Ras, Src family tyrosine kinases, eNOS, and protein kinase C isoforms (23). Accordingly, in vivo selective regulation of eNOS signaling has been demonstrated by Bucci et al. (3) in endothelial cells by using a peptide mimicking the caveolin-1 scaffolding domain (amino acids 82–101). To assess the importance of the caveolin

scaffolding domain on the regulation of the N-type Ca^{2+} channel activity we intracellularly applied the caveolin scaffolding peptide to NG108-15 cells via the recording pipette at a final concentration of 10 μM. N-currents were measured with test pulses to +10 mV, in separate populations of control- and peptide-dialyzed cells, >10 min after the break-in, to allow enough time for equilibration of the peptide within the cell interior. As shown in Fig. 1 *G*, the effect of the caveolin scaffolding peptide on the amplitude of the N-current density was negligible (−1.37 ± 0.14 pA/pF in control-dialyzed (n = 11) and −1.26 ± 0.35 in peptide-dialyzed cells (n = 11)), nor did a significant change occur in the voltage dependence of activation (not shown). These results tentatively rule out a direct regulation of N-type Ca^{2+} channel activity by interaction with the scaffolding domain of caveolin-1

Effect of cholesterol on N-currents

Caveolin-1 is known to bind newly synthesized cholesterol at the endoplasmic reticulum and to deliver it to the plasmalemma, thereby affecting membrane composition and lipid domain formation (24). Accordingly, upon measurement of cell cholesterol content, we observed a small but significant ($p < 0.01$) increase of its proportion in cav1(+) cells as compared to wild-type NG108-15 cells (0.281 ± 0.024 nmol cholesterol/nmol phospholipids in wild-type (n = 7) versus 0.32 ± 0.016 nmol cholesterol/nmol phospholipids in cav1(+) cells (n = 4)). Thus, down-regulation of basal N-type Ca^{2+} channel activity in cav1(+) cells might be a consequence of caveolin-1-induced elevation of membrane cholesterol.

Recent studies have demonstrated that cell exposure to cyclic β-cyclodextrin oligosaccharides provides a precise and reproducible method for altering cell cholesterol content (25). We applied this method to increase the cholesterol content of wild-type NG108-15 cells, thus mimicking the situation of cav1(+) cells. Total cholesterol level in NG108-15 cells that were not exposed to MβCD was 0.281 ± 0.024 nmol/nmol phospholipids (n = 7). Exposure of NG108-15 cells for 120 min to a cholesterol-saturated MβCD solution (final cholesterol concentration 5 μg/ml) resulted in a moderate but significant (p = 0.007) increase of steroid content in these cells (0.332 ± 0.036 nmol/nmol phospholipids (n = 5)). This increase is similar to the degree of cholesterol enrichment in cav1(+) cells (Fig. 2 *A*). As shown in Fig. 2 *B*, enrichment of cellular cholesterol resulted in a significant 51% decrease of N-current density measured at +10 mV (−4.28 ± 0.83 pA/pF in control NG108-15 cells (n = 18) versus −2.08 ± 0.29 pA/pF in cholesterol-enriched cells (n = 19), $p < 0.02$). The N-current density dropped to a negligible amplitude by a 10-fold increase in the concentration of exogenously applied cholesterol (final cholesterol concentration 50 μg/ml (Fig. 2 *B*), corresponding to a cell cholesterol content of 0.37 nmol cholesterol/nmol phospholipids (not shown)), thus suggesting that the degree of current depression depends on cholesterol concentration. However, cholesterol enrichment did not affect the time course of N-current activation, as shown by the sample tracings in the inset of Fig. 2 *B*. Upon fitting by single exponential functions, mean values of the activation time constant at +10 mV were, respectively, 4.4 ± 0.38 ms (n = 18) and 4.8 ± 0.45 ms (n = 19) in control and cholesterol-enriched cells. Fig. 2 *C* shows the average current-voltage relationship obtained from naïve NG108-15 cells and cells exposed to either 5 μg/ml (*solid circles*) or 50 μg/ml (*open circles*) cholesterol. It is evident that the N-current is strongly depressed within a wide range of test potentials in cholesterol-enriched cells, but no significant difference is detectable either in the activation threshold (~−30 mV), or in the peak (+10 mV) of the *I/V* relationship. The absence of significant differences in the voltage dependence of N-current activation between control and cholesterol-enriched cells was further confirmed by analyzing the shape of the normalized conductance versus voltage (Fig. 2 *D*). By contrast, we measured a significant ($p < 0.02$) decrease of maximum conductance (Fig. 1 *E*, G_{max}) from 0.087 ± 0.013 nS/pF (n = 18) to 0.044 ± 0.011 nS/pF (n = 19) in control versus cholesterol-enriched cells, respectively.

The voltage dependence of N-current inactivation was also compared for control versus cholesterol-enriched cells, using a typical double-pulse protocol, wherein a 3 s conditioning pulse to various potentials (−100/−40 mV) was followed by test steps to +10 mV. This protocol was applied to cells lacking the fast-inactivating (T-type-like) current component (~15–20% of tested cells). The voltage sensitivity of steady-state inactivation was unaltered in cholesterol-enriched cells compared to control NG108-15 cells (Fig. 2 *D*, *inset*). The $V_{½}$ for inactivation for control and cholesterol-treated cells was −60.5 mV (n = 4) and −58.5 mV (n = 3), respectively. However, it is worth noting that a shift in the voltage sensitivity of inactivation of N-type Ca^{2+} channels was reported in human neuroblastoma IMR32 cells after changes in membrane cholesterol concentration (26). Nevertheless, that effect could be observed only after chronic exposure of cells to cholesterol, and a contamination of N-current with a strong T-type Ca^{2+} current may have biased those results.

Empty MβCD can also be employed for diminishing cell cholesterol content (25). With this method it has been demonstrated that membrane cholesterol depletion has effects opposite to those of cholesterol enrichment, causing, at least in some cases and to a certain extent, an increase in ion channel current (6,15,27). To test whether the effect of caveolin expression could be suppressed by depletion of endogenous cholesterol, cav1(+) cells were incubated for 2 h in cholesterol-free MβCD at the same concentration used in cholesterol-enrichment experiments (0.1 mM). Indeed, depletion of membrane cholesterol by application of empty MβCD to cav1(+) cells resulted in an average increase (although not statistically significant, $p > 0.07$) by a factor of 1.4 of the N-current density measured at +10 mV (−1.16 ±

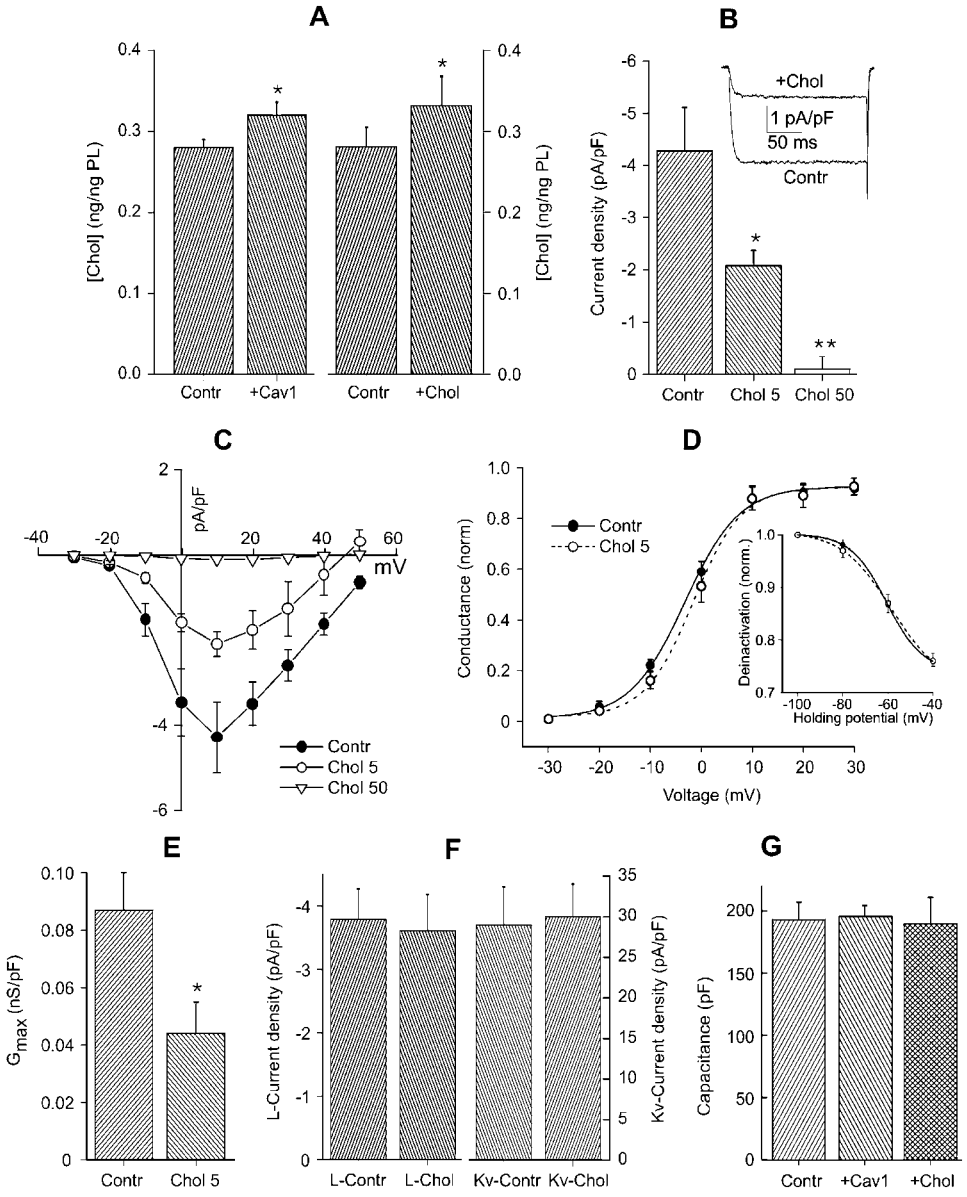

FIGURE 2 N-type Ca^{2+} channel currents in control and cholesterol-enriched NG108-15 cells. (*A*) Cholesterol content (nM/nM phospholipids) of cav1(+) (*left*), cholesterol-enriched (*right*), and wild-type NG108-15 cells (*$p < 0.01$). (*B*) Average N-current densities in control NG108-15 cells (*Contr*, $n = 18$) and in cells incubated with a MβCD/cholesterol solution (8:1 molar ratio), giving final concentrations of 5 (*Chol 5*, $n = 19$, $p < 0.02$) and 50 μg cholesterol/ml culture medium (*Chol 50*, $n = 9$, $p < 0.001$) at +10 mV. (*Inset*) Representative Ba^{2+} current density profiles obtained from a normal (*Contr*) and a cholesterol-enriched cell (5 μg cholesterol/ml; *+Chol*). Currents were elicited at +10 mV from a holding potential of −40 mV. (C) Current density-voltage relationship of N-currents from control NG108-15 (*solid symbols*, $n = 18$) and from cells enriched with 5 μg/ml (*open circles*, $n = 19$) and 50 μg/ml (*triangles*, $n = 9$) cholesterol. (*D*) Mean voltage dependence of N-type Ca^{2+} channel conductance (normalized) for control (*solid circles*, $n = 18$) and cholesterol-enriched cells (*open circles*, $n = 19$). The continuous line through data points is the least-squares best fit of the Boltzmann equation $g_{norm} = 1/\{1 + \exp[(V - V_{1/2})/k]\}$, where $V_{1/2}$ and k values were, respectively, −4 mV and 5.2 mV for control cells and −1.6 ± 0.6 mV and 4.8 ± 0.6 mV for cholesterol-enriched cells. (*Inset*) Mean N-current deinactivation versus membrane potential for control NG108-15 (*solid circles*, $n = 4$) and cholesterol-enriched cells (*open circles*, $n = 3$). Currents were elicited to +10 mV after a 3-s prepulse to the potentials indicated (−100 to −40 mV). The continuous lines through data points are the least-squares best fits of the Boltzmann equation $h = 1/\{1 + \exp[V + V_{1/2})/k]\}$, where $V_{1/2}$ and k values for the two different data sets were, respectively, 60.5 mV and 8.0 mV (control) and 58.5 mV and 11.1 mV (cholesterol-treated). (*E*) Mean N-current maximum conductances in control ($n = 18$) and cholesterol-enriched cells ($n = 19$, $p < 0.02$). (*F*) Mean current densities from L-type Ca^{2+} channels (*left*, $n = 17$) and delayed-rectifier K^+ channels (*right*, $n = 27$) in control and cholesterol-enriched cells. (*G*) Cell capacitance in control ($n = 75$), cav1(+) ($n = 96$), and cholesterol-enriched ($n = 49$) cells.

0.27 pA/pF in cav1(+) cells ($n = 12$) versus −1.82 ± 0.25 pA/pF in MβCD-cav1(+)-treated cells ($n = 10$)). The lack of a complete current recovery to values similar to those measured in control NG108-15 cells may suggest that an intense membrane cholesterol depletion, in addition to specific effects on channel activity related to those observed after cholesterol enrichment, could also cause unspecific and opposite outcomes, possibly due to plasma membrane destabilization. This hypothesis of additional unspecific effects after cholesterol depletion below physiological levels is also suggested by the following observations: 1), the seal of the patch electrode to cell membrane was generally less stable; 2), a faster Ca^{2+} channel current run-down was frequently observed; and 3), in control NG108-15 cells MβCD had no significant effect, although there was a trend for a decrease in current with MβCD. On average, in normal NG108-15 cells incubated for 2 h in cholesterol-free MβCD we measured a 16% decrease of N-current density when compared to untreated cells (−4.23 ± 0.31 pA/pF in control NG108-15 cells ($n = 15$) versus −3.59 ± 0.44 pA/pF in MβCD-treated cells ($n = 17$)). Indeed, the loss of the integrity and properties of lipid domains, accompanied by severe changes in the

membrane permeability, distress, and eventually cell death, was observed after stringent treatment with empty MβCD of cerebellar granule cells in culture (28).

To test whether cholesterol enrichment affects other conductances besides the N-type one, we measured L-type Ca^{2+} and delayed rectifier K^+ currents. The average current densities, shown in the histogram of Fig. 2 *F*, do not show any significant difference between control and cholesterol- enriched cells, suggesting that, as for caveolin-1 expression, the elevation of cellular cholesterol specifically affects the N-type current.

Altogether, the results obtained by experimentally enhancing the cholesterol concentration of wild-type NG108-15 cells are both qualitatively and quantitatively similar to those obtained from cav1(+) cells, strongly arguing in favor of the view that cholesterol enrichment mimics the effect of caveolin-1 expression and that an increase of cholesterol concentration is the cause of the observed change in N-type channel basal activity.

In principle, the whole-cell N-current can be described as the product of three factors:

$$I = N \times P_o \times I, \quad (2)$$

where N is the number of N-type channels available to opening upon depolarization; P_o, the opening probability, is a function of time and potential; and i is the unitary current. Theoretically, the size reduction of the whole-cell N-current density measured in caveolin-1-expressing cells and in cholesterol-enriched cells could arise from alterations in any of the three factors (or any combination of these factors).

Thus, to test whether caveolin-1- and cholesterol-induced decreases of N-current density could be caused by a change in the number of active channels in the plasma membrane after membrane retrieval into intracellular compartments, we tentatively estimated the total area of the membrane by measuring capacitance. It is usually assumed that the membrane bilayer is homologous to a parallel plate capacitor (29), and thus the membrane capacitance is directly proportional to the total surface area of the membrane. Measuring cell capacitance, therefore, is one of the most precise methods to determine whether membrane retrieval mechanisms are responsible for the regulation of the current density (6,30,31). If the decrease in the number of N-type channels in cholesterol-enriched and caveolin-1-expressing cells is due to membrane retrieval, then the surface of the membrane and, therefore, the membrane capacitance are expected to be decreased. However, neither changes in the levels of cholesterol nor expression of recombinant caveolin-1 have any effect on membrane capacitance of NG108-15 cells (Fig. 2 *G*). These observations might suggest that membrane retrieval mechanisms cannot explain the effect of cholesterol on density of the N-current in NG108-15 cells.

To discriminate between the two other possibilities, i.e., decrease in P_o and/or unitary current amplitude i, the effects of N-type Ca^{2+} channel inhibition by caveolin-1 expression or cholesterol enrichment were further investigated at the single-channel level.

Single N-type channel activity in cell-attached patches

All experiments in cell-attached patches were carried out with the recording pipette containing 100 mM Ba^{2+} and 10 μM nifedipine. Only under these experimental conditions could N-channel activity be well resolved, as shown in the sample tracings of Fig. 3 *A* (see also Materials and Methods). The amplitudes of unitary events were distributed around single Gaussian functions with mean amplitudes, in the voltage range between 0 mV and +40 mV, shown in Fig. 3 *B*. The channel conductance (γ) was 12 pS. The opening probability (P_o), measured by excluding null sweeps and the closed time before first opening and after last opening, was voltage-dependent with a half-maximum at +20 mV, a maximum value of 0.13 above +40 mV, and a slope of 5 mV (Fig. 3 *C*). The mean open times (t_o) and mean closed times (t_c) at various voltages, obtained from the arithmetic means of open and closed times of each patch (see Materials and Methods), were also voltage-dependent (Fig. 3 *D*). Mean t_o increased with voltage (by a factor of ~4 between 0 mV and +40 mV) whereas mean t_c decreased with increasing voltage (by a factor of ~4 between 0 mV and +40 mV). At +20 mV, mean t_o was 0.62 ± 0.05 ms ($n = 15$), which is a factor of ~1.7 smaller than that found by Lee and Elmslie (32) in sympathetic neurons.

Gating kinetics of N-type channels is modified in caveolin-1-expressing cells

The same kind of analysis was also performed using cells of the cav1(+) clone, as shown in Fig. 4. In the voltage range between 0 and +40 mV the unitary current amplitude and the average single-channel conductance (13 pS) did not significantly change in cav1(+) cells as compared to control cells (Fig. 4, *A* and *B*). This rules out the possibility that the lower N-current density measured in cav1(+) cells could be due to a decrease in single-channel conductance. Concerning P_o (Fig. 4 *C*), half-maximum potential and slope were similar to those measured in control cells (+22 mV and 6.5 mV, respectively), whereas P_o maximum value was a factor of 1.18 smaller than in control cells ($P_{max} = 0.11$). Mean t_c decreased with increasing voltage, similar to control cells, whereas mean t_o increased very weakly with voltage. For instance, at +20 mV mean t_o was 0.42 ± 0.02 ms ($n = 8$) versus 0.62 ms in control cells (Fig. 4 *D*). The slight decrease in mean t_o might correlate to the small decrease in single-channel P_o; however, by itself it would hardly justify the large N-current density decrement (>70%) measured in cav1(+) cells in the whole-cell configuration.

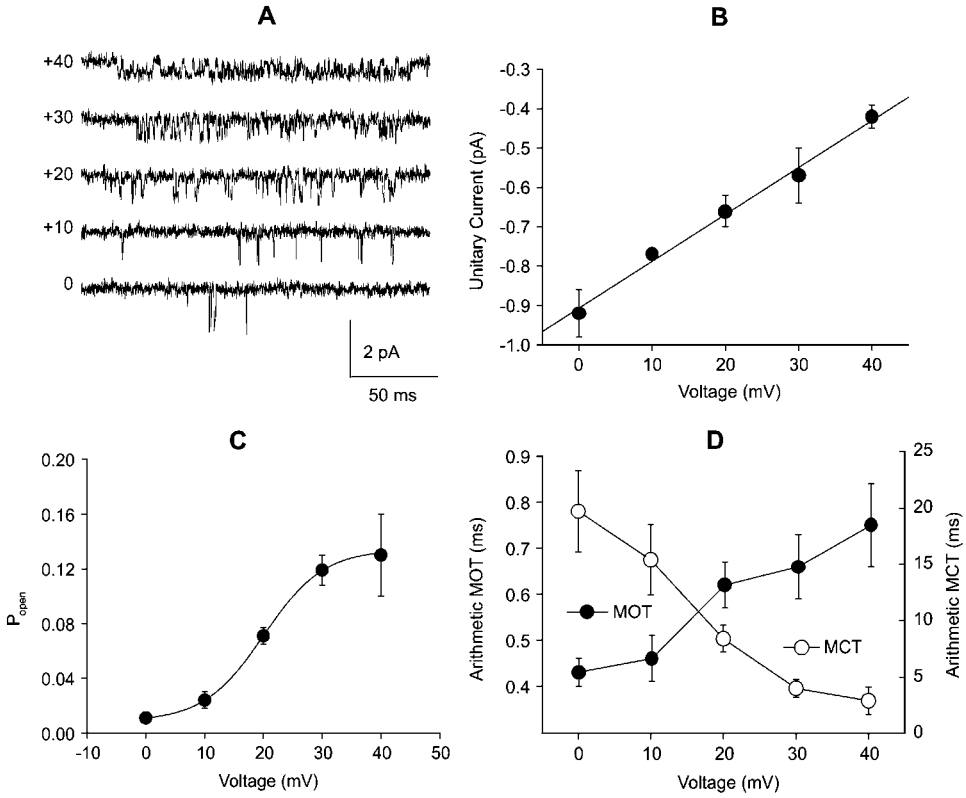

FIGURE 3 Elementary properties of single N-channels in NG108-15 cells. (*A*) Unitary N-currents were recorded between 0 and +40 mV from a holding potential of −40 mV. (*B*) Mean unitary current amplitudes plotted versus potential. The linear regression through data points has a mean slope conductance of 12 pS. (*C*) Mean open probability plotted versus potential obtained from six patches and evaluated excluding the first and last closures of the channel and null sweeps. Data points were fitted to a Boltzmann function $P_o = P_{max}/(1 + \exp((V_{1/2} - V)/k))$, where $P_{max} = 0.13$, $V_{1/2} = 20$ mV and $k = 5.1$ mV. (*D*) Mean t_o (*solid circles*, *left scale*) and mean t_c (*open circles*, *right scale*) plotted between 0 and +40 mV as obtained from six patches. The two parameters were estimated by averaging the arithmetic means of the open and closed times of each patch.

We focused our subsequent analysis on the unitary currents elicited at +20 mV test potential, where the frequency of unitary events was sufficiently high and their amplitude well distinguishable from background noise. Representative single-channel tracings, obtained by membrane depolarization to +20 mV in a control NG108-15 and a cav1(+) cell are shown in Fig. 5. Upon simple inspection and comparison between control (Fig. 5 *A*) and cav1(+) (Fig. 5 *B*) single-channel current traces, as well as between the average traces (Fig. 5, *A* and *B*, *bottom traces*), there is a clear overall reduction (69%) of N-type channel activity in the cav1(+) cell.

This decreased single-channel activity appears to arise from an increment in the time the channel spends in a nonconducting state rather than a decrement of the unitary current amplitude, whose average value is not significantly changed in cav1(+) cells (control, −0.66 ± 0.04 pA, $n = 18$; cav1(+), −0.73 ± 0.06 pA, $n = 8$).

A detailed analysis of parameters characterizing the kinetic properties of the N-type channel confirmed what was qualitatively observed by trace inspections. In Fig. 6, *A–D*, a comparison is shown between the open- and closed-time distributions obtained from the fitting of data at +20 mV in control and cav1(+) cells, respectively. Both open-time distributions were best fitted by single-exponential functions (Fig. 6, *A* and *B*), with mean open times $t_o = 0.40 \pm 0.06$ ms in control cells ($n = 8$), and $t_o = 0.27 \pm 0.02$ ms in cav1(+) cells ($n = 7$). The closed-time distributions were best fitted with two exponentials, as shown in Fig. 6, *C* and *D*, with $t_{c1} = 0.45 \pm 0.05$ ms and $t_{c2} = 9.8 \pm 1.3$ ms in control cells ($n = 8$), and $t_{c1} = 0.4 \pm 0.05$ ms and $t_{c2} = 9.7 \pm 0.7$ ms in cav1(+) cells. Thus, the major difference obtained from dwell-time analysis was a decrease by a factor of 1.5 in the mean open time in cav1(+) cells ($p < 0.05$). To test the contribution of this decrease in t_o to the overall N-current density depression (>70%), we simulated the data by substituting the rate constants calculated from the experimental kinetic parameters in a minimal three-state kinetic scheme ($C_1 \Leftrightarrow C_2 \Leftrightarrow O$). It turned out that the decrease of the mean t_o was responsible for 34% of current inhibition, thus suggesting that other processes must contribute to alter N-channel gating properties in the presence of recombinant caveolin-1.

Definitely, a significant change in response to caveolin-1 expression concerned the number of sweeps without activity. Null sweeps were found in every data set by applying test pulses to +20 mV lasting 180 ms. However, in cav1(+) cells, the percentage of null sweeps increased significantly by a factor of 6.7 ($p < 0.001$), from 6.6 ± 1.5% in control ($n = 10$) to 44.2 ± 7.5% in cav1(+) cells ($n = 7$), as shown in the histogram of Fig. 6 *E*.

The increase in null sweeps with caveolin-1 caused a consistent reduction of P_o (78%), when calculated by dividing the sum of open times by the entire step duration, i.e., including null sweeps as well as the first latency and the last closure. P_o was reduced significantly ($p < 0.001$) from 0.04

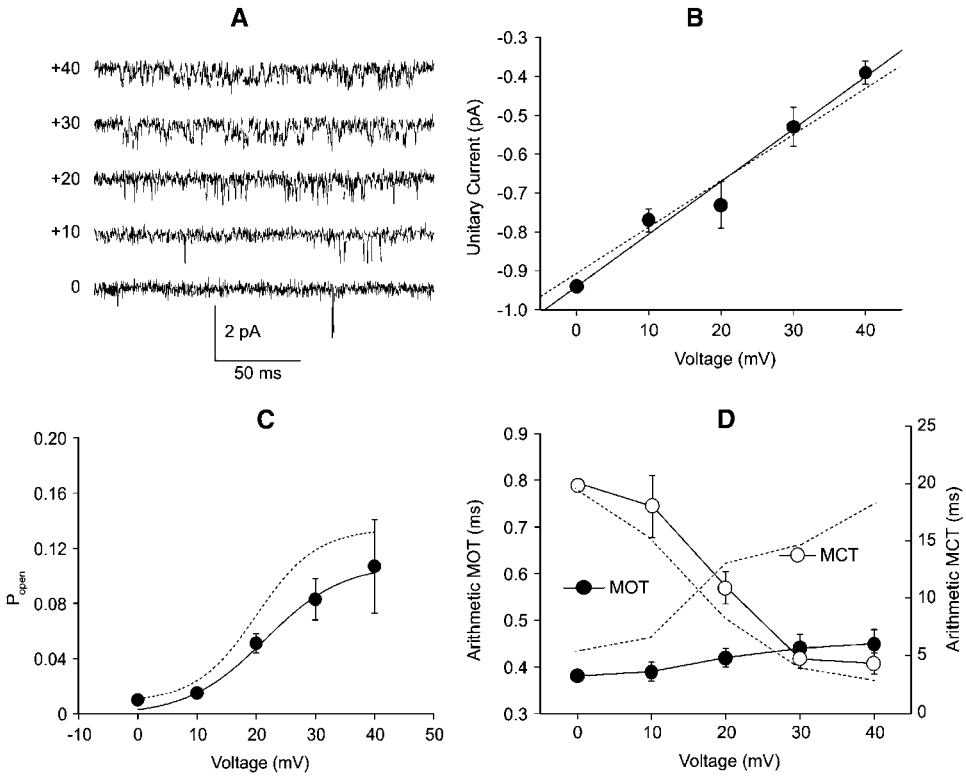

FIGURE 4 Elementary properties of single N-channels in cav1(+) cells. (*A*) Unitary N-currents were recorded between 0 and +40 mV from a holding potential of −40 mV. (*B*) Mean unitary current amplitudes plotted versus potential obtained from six patches. The linear regression through data points has a mean slope conductance of 13 pS. The dashed line represents the linear regression of control (see Fig. 3 *B*). (*C*) Mean open probability plotted versus potential obtained from six patches and evaluated excluding the first and last closures of the channel and null sweeps. Data points were fitted to a Boltzmann function $P_o = P_{max}/(1 + \exp((V_{1/2} - V)/k))$, where $P_{max} = 0.11$, $V_{1/2} = 21$ mV and $k = 6.5$ mV. The dashed line represents the control fitting curve (see Fig. 3 *C*). (*D*) Mean t_o (*solid circles*, *left scale*) and mean t_c (*open circles*, *right scale*) plotted between 0 and +40 mV as obtained from six patches. The two parameters were estimated by averaging the arithmetic means of the open and closed times of each patch. The dashed lines represent the trend of mean t_o and t_c in control NG108-15 cells (see Fig. 3 *D*).

± 0.005 in control ($n = 10$) to 0.009 ± 0.002 in cav1(+) cells ($n = 7$), as shown in the histogram of Fig. 6 *F*. Moreover, in some of these data sets, null records appeared to be clustered. We used run analysis (see Materials and Methods) to test whether the clustering of null sweeps was significant (22,32). The results reached significance in five out of six single-channel cav1(+) patches, with Z values of 1.8, 1.2, 2.5, 2.2, and 2.0. By contrast, run analysis indicated significant clustering ($Z = 0.9$ and 1.5) in only two out of seven patches in control cells, with null sweeps and active sweeps randomly mixed in the remaining five control patches.

Single N-type channel activity in cholesterol-enriched cells

Our whole-cell results indicate that a decrease in N-current density similar to that measured in cav1(+) cells could be also determined in cholesterol-enriched cells, thus suggesting that an increased cholesterol at the plasma membrane is the common denominator to both effects. Thus, we examined whether at the single-channel level cholesterol enrichment could also mimic the modifications in N-channel activity by operating on channel-gating with a mechanism similar to that displayed in cav1(+) cells. This was achieved by recording single-channel activity from cell-attached patches of cholesterol-enriched cells (incubation in 5 μg/ml for 120 min). Fig. 7 *A* shows a representative sample of five patches, where single N-channel activity was recorded at +20 mV in cholesterol-enriched cells. Also here, as with cav1(+) cells, a simple inspection of the average trace (Fig. 7 *A*, *bottom trace*), and a comparison with that obtained under control conditions (Fig. 5 *A*, *bottom trace*) indicates an overall reduction of N-type channel activity (57%) after cholesterol enrichment, which, however, does not arise from a decrement of the unitary current amplitude, whose average value does not shift significantly from that of control (−0.71 ± 0.05 pA, $n = 6$). Also for cholesterol-enriched cells, the open-time distribution obtained at +20 mV from five cells was best fitted by a single-exponential function with mean $t_o = 0.23$ ± 0.03 ms (Fig. 6 *B*), and the closed-time distribution by two exponentials, with means $t_{c1} = 0.31$ ± 0.04 ms and $t_{c2} =$ 8.7 ± 1.6 ms (Fig. 6 *C*). Thus, in cholesterol-enriched cells, besides an increase in t_o, an enhanced number of null sweeps and, consequently, reduced P_o (Fig. 7, *D* and *E*) were also significantly different from control cells. After cholesterol treatment, the percentage of null sweeps increased by a factor of 8 ($p < 0.001$) to 53.4 ± 4.9% ($n = 6$), whereas P_o (including null sweeps) was significantly reduced by 60% ($p < 0.002$) to 0.016 ± 0.004 ($n = 6$). Moreover, also in cholesterol-enriched patches, null records appeared to be clustered. By run analysis we found that clustering of null sweeps was significant in five out of six single-channel patches, with Z values 0.15, 1.37, 0.29, 1.85, and 0.67.

DISCUSSION

The main findings of this study are that 1), N-type Ca^{2+} channel activity is down-modulated and cholesterol content

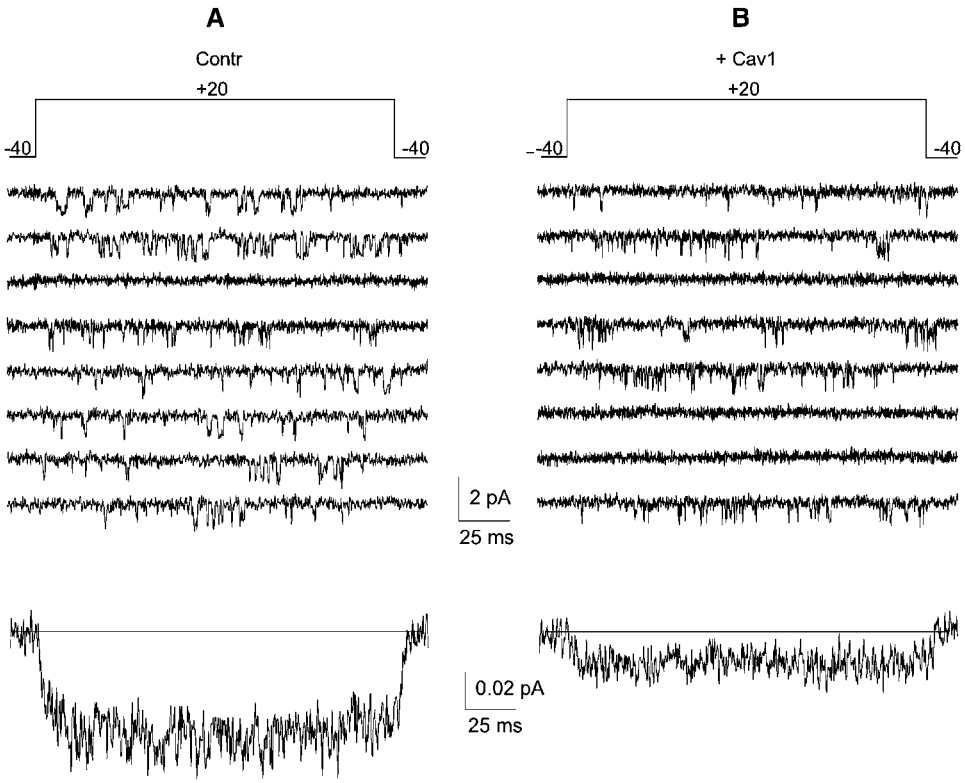

FIGURE 5 Representative traces of single N-channel activity recorded from cell-attached patches of control NG108-15 and cav1(+) cells. (*A*) Traces from a control NG108-15 cell obtained with pulses from −40 to +20 mV of 180 ms each. The averaged current at the bottom (−0.051 pA) was calculated over 257 sweeps including nulls. (*B*) Traces from a cav1(+) cell. The averaged current at the bottom is 69% smaller (−0.016 pA) than control (423 sweeps including nulls). The patch pipette contained 100 mM Ba^{2+} and the L-type Ca^{2+} channel blocker nifedipine (10 μM).

is increased in cav1(+) NG108-15 cells; 2), N-type channel down-modulation is mimicked by enhancement of membrane cholesterol with exogenous addition. By combining whole-cell and single-channel recordings we have provided evidence that a common mechanism underlies N-type Ca^{2+} channel down-modulation caused by either caveolin-1 expression or direct cholesterol enhancement.

There is evidence that the gating properties of several ion channels, e.g., $K_V1.5$ channel, specifically targeted to caveolae, are modified by changes in the caveolar microenvironment (33). In addition, caveolins, which are typically the main cytoplasmic coat proteins of caveolae, have been involved as negative regulators of signal transduction through the binding of the ''scaffolding domain'' to key signaling molecules (23). We have previously demonstrated that in cav1(+) cells the N-current density is ~70% lower than in wild-type NG108-15 cells. By analogy to reports about the interaction of signaling molecules with caveolins, we first hypothesized that N-current inhibition might have been caused by direct binding of the N-type channel to the scaffolding domain of caveolin-1. Although the data presented here do not rule out the physiological importance of direct caveolin interaction in signaling, they make unlikely a direct role of the scaffolding domain in the down-regulation of N-type Ca^{2+} channel activity. An alternative mechanism for caveolin-1-mediated N-current depression is suggested by the known role of caveolins as cholesterol-binding proteins to deliver newly synthesized cholesterol from the endoplasmic reticulum to the plasmalemma. Regulation of transmembrane signal transduction may thus occur indirectly, as a consequence of a change in the membrane and/or domain properties (24).

Indeed, the exogenous addition of cholesterol not only increased cholesterol in wild-type NG108-15 cells to the same extent as that observed in cav1(+) cells, but also lowered the N-current in a concentration-dependent manner, with features very similar to those observed in cav1(+) cells. The effect of cholesterol was specific for N-type Ca^{2+} channels, as neither L-type Ca^{2+} current nor delayed-rectifier K^+ current were significantly affected in cholesterol-enriched NG108-15 cells (Figs. 1 *F* and 2 *G*). Our finding that cholesterol enrichment results in a specific effect rather than a nonspecific alteration of membrane protein functions is corroborated by the observation that also in isolated gallbladder smooth muscle cells cholesterol significantly attenuated voltage-gated calcium currents without affecting voltage-activated outward K^+ currents (34). Furthermore, a membrane cholesterol selective modulation of L-type but not T-type channel currents in skeletal muscle cells (31) and in coronary artery smooth muscle cells (27) has been reported.

It is not surprising that ion channels, i.e., proteins specifically designed to overcome membrane impermeability, might be functionally affected by changes in the lipid composition of the membrane. Accordingly, the depletion or enrichment of lipids significantly affects the function of a number of channel types, translating into large changes of cellular excitability (5,33–35). However, it is unclear how

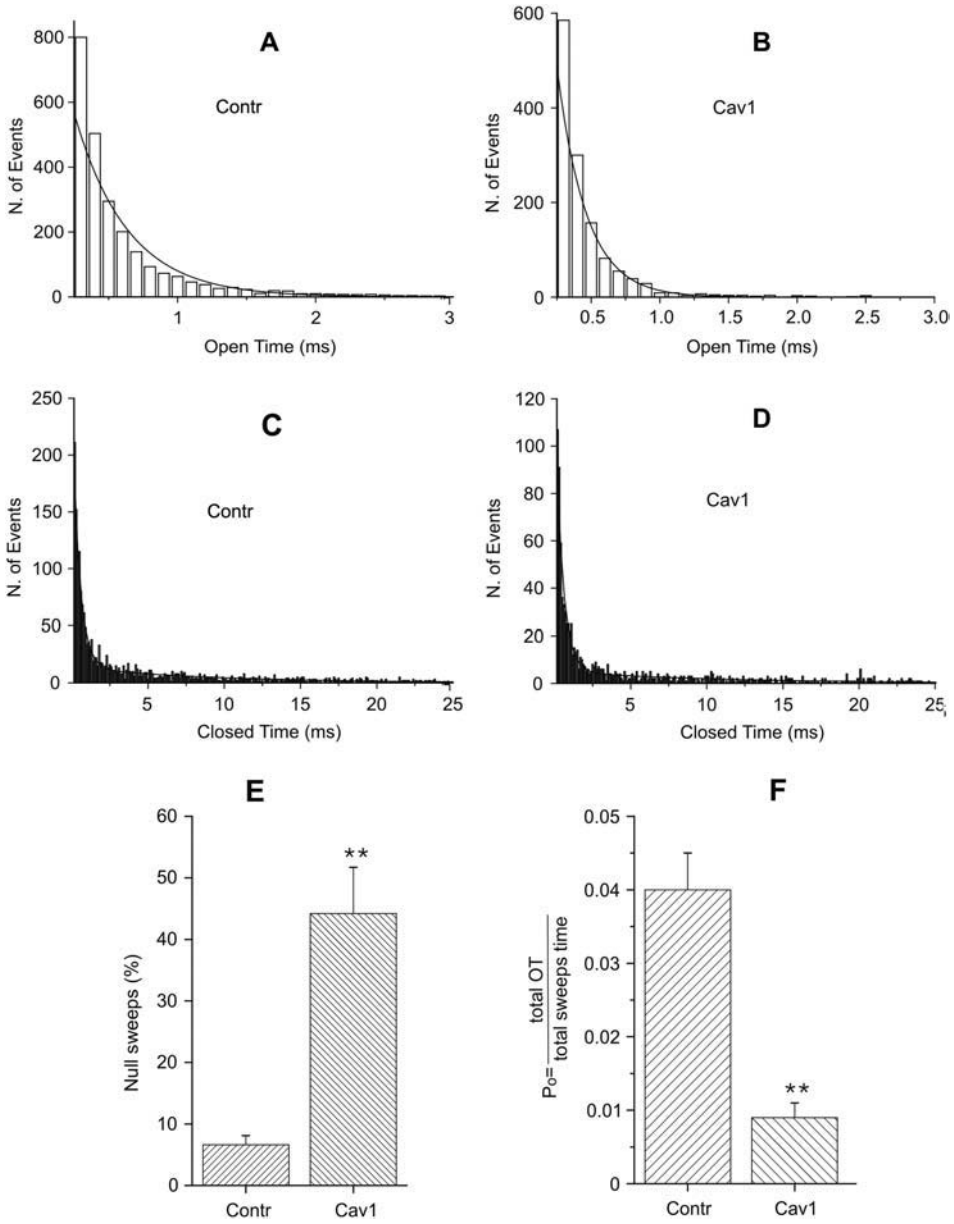

FIGURE 6 In cav1(+) cells the kinetics of gating is modified. (*A–D*) Open- and closed-time distributions at +20 mV were obtained by pooling together all single-channel events from control (*A* and *C*) and cav1(+) cells (*B* and *D*). Open and closed distributions were fitted by one and two exponential functions, respectively (*continuous curves*). The calculated mean open and closed times were as follows: control, $t_o = 0.38$, $t_{c1} = 0.5$, $t_{c2} = 8.8$; cav1(+), $t_o = 0.21$, $t_{c1} = 0.5$, $t_{c2} = 9.8$. (*E*) Mean percentage of null sweeps derived from 10 control patches and from seven cav1(+) patches ($p < 0.001$). (*F*) P_o values, calculated by dividing the sum of open times by the entire step duration including null sweeps, from 10 patches (control) and seven patches (cav1(+), $p < 0.001$), respectively.

changes in membrane cholesterol can directly modulate ion channel function, and different mechanisms have been postulated. Concerning the N-type Ca^{2+} channel, only the amplitude of the macroscopic current elicited in the whole-cell configuration seems to be affected by cholesterol enhancement, without significant changes in the voltage dependence or kinetics of activation and inactivation.

The whole-cell N-current amplitude can be described as the product of three factors: the total number of N-type channels, the unitary current amplitude, and the opening probability, which in turn depends both on the fraction of the active channels, i.e., channels available to opening during a depolarization, and on the probability that an active channel will be open. Since the single-channel conductance does not change significantly in caveolin-expressing and cholesterol-enriched cells when compared to control NG108-15 cells (Fig. 4 *B*), we can exclude the possibility that the size reduction of the whole-cell N-current density measured in caveolin-expressing and cholesterol-enriched cells could arise from a decrease in the unitary current. Rather than causing changes in the basic pore properties, membrane cholesterol seems to affect the number of active N-channels in the membrane by regulating the equilibrium between the open and closed states of these channels. What mechanism(s) could be responsible for this regulation? It is unlikely that the expression of the genes coding for the α_1, β, and α_2-δ subunits of the N-channel is under regulation by the cellular cholesterol level, because a significant down-regulation of the current was observed 2 h after application of exogenous cholesterol. This period is much shorter than the typical time

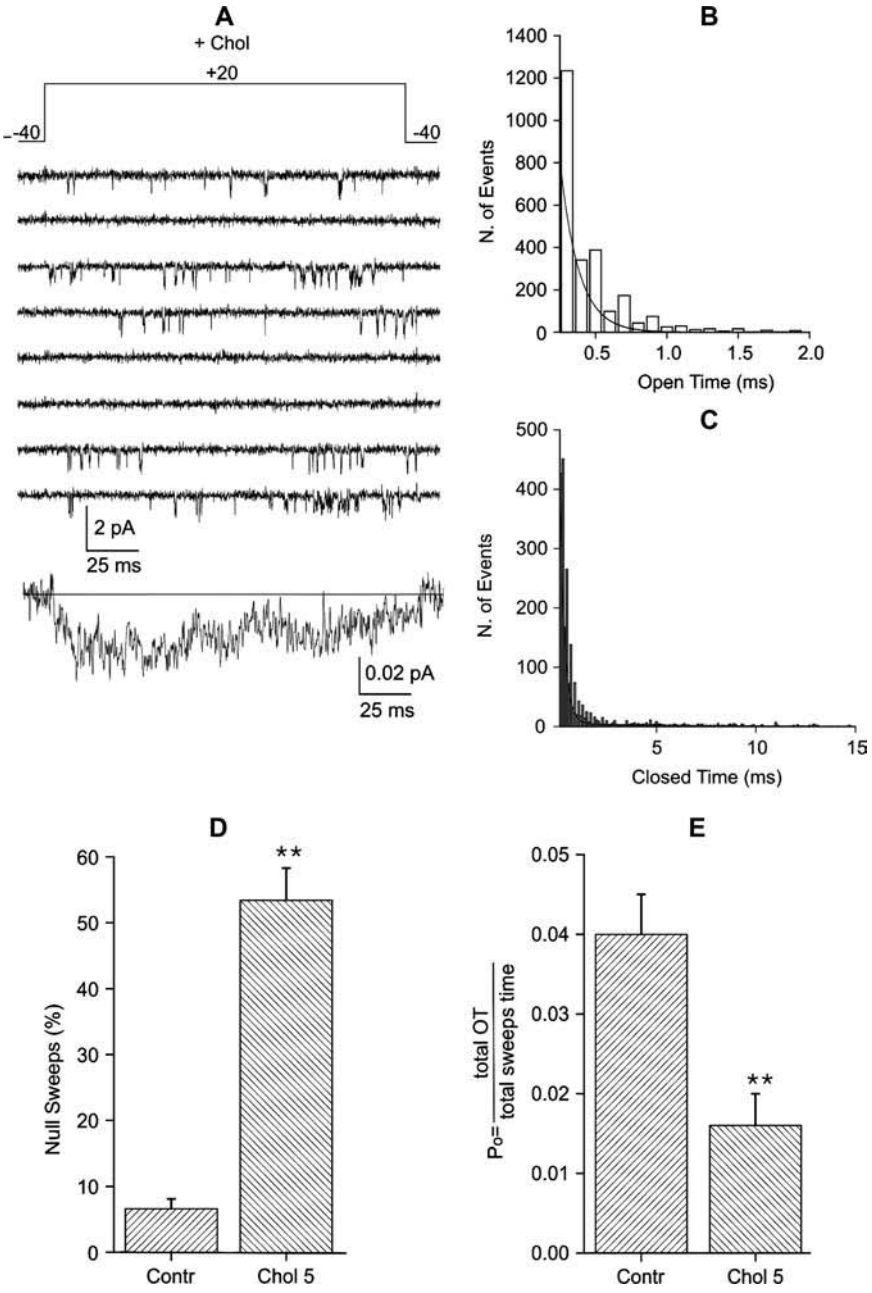

FIGURE 7 N-type channel gating modifications by caveolin-1 expression are mimicked by cholesterol enhancement in NG108-15 cells. (*A*) Representative traces of N-type channel activity recorded at +20 mV from a cell-attached patch after cholesterol enrichment. The averaged current at the bottom (−0.022 pA), calculated over 198 sweeps including null sweeps, displays lower amplitude than control one (−0.051 pA; see Fig. 5 *A*). (*B* and *C*) Open- and closed-time distributions at +20 mV were obtained by pooling together all single-channel events from cholesterol-enriched cells. Open and closed distributions were fitted by one and two exponential functions, respectively (*continuous curves*). The calculated mean open and closed times were as follows: $t_o = 0.22$, $t_{c1} = 0.38$, and $t_{c2} = 8.2$. (*D*) Mean percentage of null sweeps derived from 10 control patches and from six cholesterol-enriched patches ($p < 0.001$). (*E*) P_o values, calculated by dividing the sum of open times by the entire step duration including null sweeps, from 10 (*Contr*) and six patches (*Chol 5*, $p < 0.002$), respectively.

course expected for changes in N-channel gene expression. When N-type channel subunits are heterologously expressed in *Xenopus* oocytes or COS-7 cells by cDNA injection or transfection, a 24- to 48-h incubation is typically necessary to attain a maximal channel activity (36). Thus, we conclude that the relatively short time needed for the N-current to respond to a cholesterol change and to reach a new steady state suggests that the regulation of the N-channels is not a consequence of a change in the level of expression of the channel.

Another possibility is that the decrease in the number of active channels may be a result of the retrieval of plasma membrane into intracellular compartments. This mechanism has been proposed to explain the modulation of Kir 2.1 channels by tyrosine phosphorylation, because the tyrosine kinase-induced decrease in Kir 2.1 current density was accompanied by a significant decrease in membrane capacitance (37). Our observations show, however, that cholesterol enrichment after either exogenous application or expression of recombinant caveolin-1 is not accompanied by a decrease in cell capacitance, indicating that alterations in the membrane cholesterol composition do not cause major changes in the surface area. Interestingly, however, other researchers have found changes in membrane capacitance

after cholesterol sequestering by exposure to MβCD (31). In conclusion, although we cannot completely exclude the possibility that the sterol composition of the membrane regulates the retrieval of the plasma membrane and the fusion of small intracellular vesicles, which contain N-type but not other types of ion channels, our data tentatively suggest that membrane retrieval is not likely to account for the cholesterol-induced regulation of N-channels.

The mechanism of the tonic, steady-state depression of the whole-cell N-current after cholesterol enhancement could be further dissected by single-channel analysis. One major difference, found by the analysis of kinetic parameters, was a decrease in the mean open time, which, according to our simulations, could be responsible for an overall N-current decrease of ~30%. Indeed, earlier studies have shown that an increase in membrane cholesterol content reduced the open probability of Ca^{2+}-dependent K^+ channels (38,39) and of VRAC channels (15). We identified another property that consistently reduced P_o in response to cholesterol enhancement, and this was an increase in the null sweeps. Specifically, null sweeps were significantly clustered in the majority of our single N-channel patches enriched in cholesterol after either expression of recombinant caveolin-1 or cell treatment with exogenous cholesterol. Clustering of null records has been reported for N-type calcium channels (32), skeletal muscle sodium channels (22), and L-type Ca^{2+} channels (40). These observations led us to the hypothesis that clustered null sweeps result from a mode of N-channel gating from which the channel will not open (null P_o mode), and therefore show an overall temporary decrease in the fraction of active channels.

A classical model predicts channel activities that have a homogeneous gating pattern characterized by one set of kinetic parameter values (gating mode). Single-channel recordings, however, have shown that Ca^{2+} channel activity may derive from a discrete number of gating modes, distinguished by their opening probabilities. Switching to different gating modes with significantly different mean $\underline{P}_o$ has been observed for both the N-type (32) and the L-type Ca^{2+} channels (40). If we assume that after cholesterol loading channels exhibit a long (hundreds of milliseconds) stay in the null P_o mode, this would make the transition from null to normal P_o mode rather unlikely for intervals of ~180 ms, which was the duration of our sweeps. This would produce assemblies of smaller-sized currents with time courses similar to those of control currents, as we observed in the whole-cell configuration. In turn, at the single-channel level, this would originate a sizeable increase in the null sweeps, as we observed in the cell-attached configuration. In this sense our results seem to be very similar to those obtained for Kir channels in endothelial cells (6), although the authors interpreted their observations in terms of the existence of two subpopulations of channels: active channels that flicker between closed and open states, and silent channels that stabilize in the closed state. It was hypothesized that regulation of the Kir channels by cholesterol was mediated by a shift in the distribution between the active and silent subpopulations of the channels in the plasma membrane. An increase in null sweeps was also observed during autocrine inhibition of L-type Ca^{2+} channels in chromaffin cells (41).

The question remains as to how a change in cell cholesterol shifts the channel from a high P_o to a null P_o gating mode. It has been suggested that the suppression of channel activity by an increase in membrane cholesterol is due to an increase in membrane deformation energy that is associated with the transition between the closed and open states of the channel (15). If such a transition perturbs the membrane lipid bilayer by a change in the protein hydrophobic length, then the membrane is stiffer and the energy cost of the transition is larger (26). Elevation of the membrane cholesterol level alters the mechanical properties of the membrane bilayer, resulting in increased membrane stiffness and, consequently, in enhanced membrane deformation energy associated with channel opening (26). Therefore, if membrane deformation energy significantly contributes to the overall energy requirement for channel activation, an increase in membrane cholesterol is expected to suppress current activation. Accordingly, changes in the physical properties of the membrane (e.g., membrane stiffness) are of primary importance. This hypothesis may be related to the demonstrated mechanosensitivity of N-type calcium channels, whose gating properties are modified by stretch, i.e., by changes in membrane tension (42). Otherwise, the channel functional changes could be due to direct effects of the altered lipid composition on channel activity, since charged lipids contribute a surface potential. However, the magnitude of an effect of altered bilayer charge on potential-dependent channel parameters remains unknown. Also, we cannot exclude the possibility that membrane cholesterol may affect the intrinsic activation energy of the channel protein through specific sterol-protein interactions. This will be addressed in our further studies by the structural analysis of the effects of cholesterol analogs on N-type channel activation.

Another potential role for cellular lipids is in the regulation of channel localization. The existence of membrane microdomains rich in sphingolipids and cholesterol, particularly those referred to as lipid rafts and caveolae, has been involved in the membrane assembly of a number of signaling complexes. Several ion channels localize to lipid rafts (4) and raft association could primarily serve to assemble signaling proteins with ion channels (23). Many channel types are modulated by the activation of various signal transduction pathways and contain multiple phosphorylation sites. For instance, several reports suggest that the proximity of a tyrosine kinase with the K_V channel substrate is important for phosphorylation (4). More importantly, this compartmentalization may also provide a regulatory mechanism, as for the proximity of channels with lipid second messengers such as phosphatidylinositol (4,5)-bisphosphate, which directly and dramatically modulates channel activity (43).

The authors thank Dr. W. C. Sessa from the Dept. of Pharmacology of Yale University School of Medicine for the generous gift of the caveolin scaffolding-domain peptide.

This work was supported by grants from the Italian Ministry for Instruction, University and Research (MIUR) to M.T. (FIRB 2001 No. RBAU 01XWS4_002 and PRIN 2004 No. 2004052155_002) and M.P. (FIRB 2001 No. RBAU01XWS4_001).

REFERENCES

1. Li, S., J. Couet, and M. P. Lisanti. 1996. Src tyrosine kinases, G alpha subunits, and H-Ras share a common membrane-anchored scaffolding protein, caveolin. Caveolin binding negatively regulates the auto-activation of Src tyrosine kinases. *J. Biol. Chem.* 271:29182–29190.
2. Razani, B., C. S. Rubin, and M. P. Lisanti. 1999. Regulation of cAMP-mediated signal transduction via interaction of caveolins with the catalytic subunit of protein kinase A. *J. Biol. Chem.* 274:26353–26360.
3. Bucci, M., J. P. Gratton, R. D. Rudic, L. Acevedo, F. Roviezzo, G. Cirino, and W. C. Sessa. 2000. In vivo delivery of the caveolin-1 scaffolding domain inhibits nitric oxide synthesis and reduces inflammation. *Nat. Med.* 6:1362–1367.
4. Martens, J. R., K. O'Connell, and M. Tamkun. 2004. Targeting of ion channels to membrane microdomains: localization of KV channels to lipid rafts. *Trends Pharmacol. Sci.* 25:16–21.
5. Martens, J. R., R. Navarro-Polanco, E. A. Coppock, A. Nishiyama, L. Parshley, T. D. Grobaski, and M. M. Tamkun. 2000. Differential targeting of Shaker-like potassium channels to lipid rafts. *J. Biol. Chem.* 275:7443–7446.
6. Romanenko, V. G., Y. Fang, F. Byfield, A. J. Travis, C. A. Vandenberg, G. H. Rothblat, and I. Levitan. 2004. Cholesterol sensitivity and lipid raft targeting of Kir2.1 channels. *Biophys. J.* 87: 3850–3861.
7. Hajdu, P., Z. Varga, C. Pieri, G. Panyi, and R. Gaspar, Jr. 2003. Cholesterol modifies the gating of Kv1.3 in human T lymphocytes. *Pflugers Arch.* 445:674–682.
8. Tillman, T., and M. Cascio. 2003. Effects of membrane lipids on ion channel structure and function. *Cell Biochem. Biophys.* 38:161–190.
9. Toselli, M., V. Taglietti, V. Parente, S. Flati, A. Pavan, F. Guzzi, and M. Parenti. 2001. Attenuation of G protein-mediated inhibition of N-type calcium currents by expression of caveolins in mammalian NG108–15 cells. *J. Physiol.* 536:361–373.
10. Galbiati, F., D. Volonté, O. Gil, G. Zanazzi, J. L. Salzer, M. Sargiacomo, P. E. Scherer, J. A. Engelman, A. Schlegel, M. Parenti, T. Okamoto, and M. P. Lisanti. 1998. Expression of caveolin-1 and -2 in differentiating PC12 cells and dorsal root ganglion neurons: caveolin-2 is up-regulated in response to cell injury. *Proc. Natl. Acad. Sci. USA.* 95:10257–10262.
11. Braun, J. E. A., and D. V. Madison. 2000. A novel SNAP25-caveolin complex correlates with the onset of persistent synaptic potentiation. *J. Neurosci.* 20:5997–6006.
12. Gorodinsky, A., and D. A. Harris. 1995. Glycolipid-anchored proteins in neuroblastoma cells form detergent-resistant complexes without caveolin. *J. Cell Biol.* 129:619–627.
13. Kasai, H., and E. Neher. 1992. Dihydropyridine-sensitive and ω-conotoxin-sensitive calcium channels in a mammalian neuroblastoma-glioma cell line. *J. Physiol.* 448:161–188.
14. Sternberg, P. W., and S. L. Schmid. 1999. Caveolin, cholesterol and Ras signalling. *Nat. Cell Biol.* 1:E35–E37.
15. Levitan, I., A. E. Christian, T. N. Tulenko, and G. H. Rothblat. 2000. Membrane cholesterol content modulates activation of volume-regulated anion current in bovine endothelial cells. *J. Gen. Physiol.* 115:405–416.
16. Giglioni, A., M. Pitto, V. Chigorno, L. Zorzino, and R. Guidoni. 1990. Subcellular metabolism of exogenous GM1 ganglioside in normal human fibroblasts. *Biochem. Int.* 22:85–94.
17. Peterson, G.L. (1977) A simplification of the protein assay method of Lowry et al. which is more generally applicable. *Anal. Biochem.* 83: 346–356.
18. Tsunoo, A., M. Yoshii, and T. Narahashi. 1986. Block of calcium channels by enkephalin and somatostatin in neuroblastoma-glioma hybrid NG108–15 cells. *Proc. Natl. Acad. Sci. USA.* 83:9832–9836.
19. Plummer, M. R., D. E. Logothetis, and P. Hess. 1989. Elementary properties and pharmacological sensitivities of calcium channels in mammalian peripheral neurons. *Neuron.* 2:1453–1463.
20. Colquhoun, D., and A. G. Hawkes. (1995). The principles of the stocastic interpretation of ion-channel mechanisms. *In* Single Channel Recording. B. Sackmann and E. Neher, editors. Plenum Press, New York. 397–482.
21. Sigworth, F. J., and S. M. Sine. 1987. Data transformations for improved display and fitting of single-channel dwell time histograms. *Biophys. J.* 52:1047–1054.
22. Horn, R., C. A. Vandenberg, and K. Lange. 1984. Statistical analysis of single sodium channels: effects of N-bromoacetamide. *Biophys. J.* 45:323–335.
23. Okamoto, T., A. Schlegel, P. E. Scherer, and M. P. Lisanti. 1998. Caveolins, a family of scaffolding proteins for organizing ''pre-assembled signaling complexes'' at the plasma membrane. *J. Biol. Chem.* 273:5419–5422.
24. Smart, E. J., Y. Ying, W. C. Donzell, and R. G. Anderson. 1996. A role for caveolin in transport of cholesterol from endoplasmic reticulum to plasma membrane. *J. Biol. Chem.* 271:29427–29435.
25. Christian, A. E., M. P. Haynes, M. C. Phillips, and G. H. Rothblat. 1997. Use of cyclodextrins for manipulating cellular cholesterol content. *J. Lipid Res.* 38:2264–2272.
26. Lundbaek, J. A., P. Birn, A. J. Hansen, and O. S. Andersen. 1996. Membrane stiffness and channel function. *Biochemistry.* 35:3825–3830.
27. Bowles, D. K., C. L. Heaps, J. R. Turk, K. K. Maddali, and E. M. Price. 2004. Hypercholesterolemia inhibits L-type calcium current in coronary macro-, not microcirculation. *J. Appl. Physiol.* 96:2240–2248.
28. Ottico, E., A. Prinetti, S. Prioni, C. Giannotta, L. Basso, V. Chigorno, and S. Sonnino. 2003. Dynamics of membrane lipid domains in neuronal cells differentiated in culture. *J. Lipid Res.* 44:2142–2151.
29. Hille, B. (1992) Ionic Channels in Excitable Membranes, 2nd ed. Sinauer Associates, Sunderland, MA.
30. Penner, R., and E. Neher. 1989. The patch-clamp technique in the study of secretion. *Trends Neurosci.* 12:159–163.
31. Pouvreau, S., C. Berthier, S. Blaineau, J. Amsellem, R. Coronado, and C. Strube. 2004. Membrane cholesterol modulates dihydropyridine receptor function in mice fetal skeletal muscle cells. *J. Physiol.* 555: 365–381.
32. Lee, H. K., and K. S. Elmslie. 1999. Gating of single N-type calcium channels recorded from bullfrog sympathetic neurons. *J. Gen. Physiol.* 113:111–124.
33. Martens, J. R., N. Sakamoto, S. A. Sullivan, T. D. Grobaski, and M. M. Tamkun. 2001. Isoform-specific localization of voltage-gated K+ channels to distinct lipid raft populations. Targeting of Kv1.5 to caveolae. *J. Biol. Chem.* 276:8409–8414.
34. Jennings, L. J., Q. W. Xu, A. F. Tracy, T. N. Mark, and G. M. Mawe. 1999. Cholesterol inhibits spontaneous action potentials and calcium currents in guinea pig gallbladder smooth muscle. *Am. J. Physiol.* 277:G1017–G1026.
35. Barbuti, A., B. Gravante, M. Riolfo, R. Milanesi, B. Terragni, and D. Di Francesco. 2004. Localization of pacemaker channels in lipid rafts regulates channel kinetics. *Circ. Res.* 94:1325–1331.
36. Canti, C., K. M. Page, G. J. Stephens, and A. C. Dolphin. 1999. Identification of residues in the N terminus of α1B critical for inhibition of the voltage-dependent calcium channel by G$\beta\gamma$. *J. Neurosci.* 19:6855–6864.
37. Tong, Y., G. S. Brandt, M. Li, G. Shapovalov, E. Slimko, A. Karschin, D. A. Dougherty, and H. A. Lester. 2001. Tyrosine

decaging leads to substantial membrane trafficking during modulation of an inward rectifier potassium channel. *J. Gen. Physiol.* 117: 103–118.

38. Bolotina, V., V. Omelyanenko, B. Heyes, U. Ryan, and P. Bregestovski. 1989. Variations of membrane cholesterol alter the kinetics of Ca^{2+}-dependent K^+ channels and membrane fluidity in vascular smooth muscle cells. *Pflugers Arch.* 415:262–268.
39. Chang, H. M., R. Reitstetter, R. P. Mason, and R. Gruener. 1995. Attenuation of channel kinetics and conductance by cholesterol: an interpretation using structural stress as a unifying concept. *J. Membr. Biol.* 143:51–63.
40. Hess, P., J. B. Lansman, and R. W. Tsien. 1984. Different modes of Ca channel gating behaviour favoured by dihydropyridine Ca agonists and antagonists. *Nature.* 311:538–544.
41. Carabelli, V., J. M. Hernandez-Guijo, P. Baldelli, and E. Carbone. 2001. Direct autocrine inhibition and cAMP-dependent potentiation of single L-type Ca^{2+} channels in bovine chromaffin cells. *J. Physiol.* 532:73–90.
42. Calabrese, B., I. V. Tabarean, P. Juranka, and C. E. Morris. 2002. Mechanosensitivity of N-type calcium channel currents. *Biophys. J.* 83:2560–2574.
43. Hilgemann, D. W. 2004. Oily barbarians breach ion channel gates. *Science.* 304:223–224.